Science of the Total Environment 712 (2020) 136450

Contents lists available at ScienceDirect

Science of the Total Environment

journal homepage: www.elsevier.com/locate/scitotenv

Development of a quantitative structure-activity relationship model for mechanistic interpretation and quantum yield prediction of singlet oxygen generation from dissolved organic matter

Jianchen Zhao [a], Yangjian Zhou [a], Chao Li [a], Qing Xie [b], Jingwen Chen [b], Guangchao Chen [c], Willie J.G.M. Peijnenburg [c,d], Ya-nan Zhang [a,*], Jiao Qu [a,*]

[a] State Environmental Protection Key Laboratory of Wetland Ecology and Vegetation Restoration, School of Environment, Northeast Normal University, Changchun 130117, China
[b] Key Laboratory of Industrial Ecology and Environmental Engineering (MOE), School of Environmental Science and Technology, Dalian University of Technology, Dalian 116024, China
[c] Institute of Environmental Sciences, Leiden University, Leiden, the Netherlands
[d] National Institute of Public Health and the Environment (RIVM), Center for Safety of Substances and Products, Bilthoven, the Netherlands

HIGHLIGHTS

- Quantum yields of $^1O_2$ from DOM-analogs, sensitizers, and SRFA were determined.
- Multiple linear regression based QSAR-model for Φ_{1O2} was constructed.
- The constructed QSAR-model exhibited satisfactory goodness-of-fit and robustness.
- Underlying mechanisms of $^1O_2$ generation were discussed based on molecular descriptors.
- The constructed QSAR model was successfully used to predict Φ_{1O2} value of SRFA.

GRAPHICAL ABSTRACT

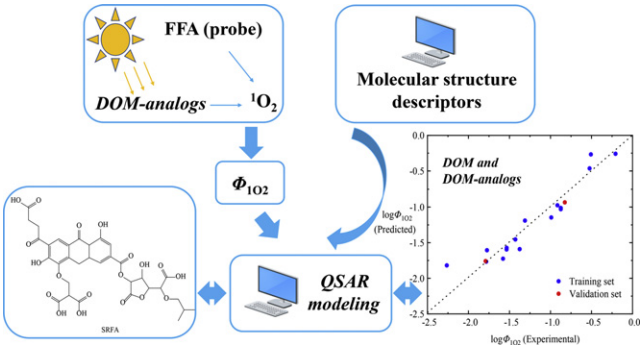

ARTICLE INFO

Article history:
Received 28 October 2019
Received in revised form 29 December 2019
Accepted 30 December 2019
Available online 7 January 2020

Editor: Yolanda Picó

Keywords:
Singlet oxygen
Quantum yield
Quantitative structure-activity relationship
Dissolved organic matter

ABSTRACT

Singlet oxygen ($^1O_2$) is capable of degrading organic contaminants and inducing cell damage and inactivation of viruses. It is mainly generated through the interaction of dissolved oxygen with excited triplet states of dissolved organic matter (DOM) in natural waters. The present study aims at revealing the underlying mechanism of $^1O_2$ generation and providing a potential tool for predicting the quantum yield of $^1O_2$ (Φ_{1O2}) generation from DOM by constructing a quantitative structure-activity relationship (QSAR) model. The determined Φ_{1O2} values for the selected DOM-analogs range from $(0.54 \pm 0.23) \times 10^{-2}$ to $(62.03 \pm 2.97) \times 10^{-2}$. A QSAR model was constructed and was proved to have satisfactory goodness-of-fit and robustness. The QSAR model was successfully used to predict the Φ_{1O2} of Suwannee River fulvic acid. Mechanistic interpretation of the descriptors in the model showed that hydrophobicity, molecular complexity and the presence of carbonyl groups in DOM play crucial roles in the generation of $^1O_2$ from DOM. The presence of other heteroatoms besides O, such as N and S, also affects the generation of $^1O_2$. The results of this study provide valuable insights into the generation of $^1O_2$ from DOM in sunlit natural waters.

* Corresponding authors.
E-mail addresses: zhangyn912@nenu.edu.cn (Y. Zhang), quj100@nenu.edu.cn (J. Qu).

https://doi.org/10.1016/j.scitotenv.2019.136450
0048-9697/

1. Introduction

The presence of singlet oxygen ($^1O_2$) in surface waters has attracted much attention due to its important role in chemical and biological processes in the environment (Mostafa and Rosario-Ortiz, 2013; Peterson et al., 2012). Singlet oxygen is a non-radical and an electrophilic oxidant that selectively reacts with electron-rich moieties of organic compounds (Agnez-Lima et al., 2012). As a consequence, $^1O_2$ is reported to play an important role in the degradation of organic contaminants containing phenolic, sulfidic, or olefinic moieties in natural waters (Appiani et al., 2017; Vione et al., 2014). For example, $^1O_2$ has been proven to be involved in the photodegradation of antibiotics (Niu et al., 2016), fibrate drugs (Zhang et al., 2018b), chlorophenolates (Czaplicka, 2006), and many other well-known micro-pollutants (Karpuzcu et al., 2016; Xie et al., 2013) in sunlit surface waters. Besides, the high reactivity of $^1O_2$ with biological macromolecules (nucleic acids, amino acids, and lipids) makes it a potent reactant to induce DNA damage and to inactivate health-relevant microorganisms in water (Cadet et al., 2008; Nelson et al., 2018; Straight and Spikes, 1985).

Dissolved organic matter (DOM) is ubiquitous in natural waters, and plays a crucial role in the generation of $^1O_2$ (Latch and McNeill, 2006; Zepp et al., 1977). Singlet oxygen is generated through the energy transfer reaction from the excited triplet state of DOM ($^3DOM^*$) to dissolved molecular oxygen (O_2) (Foote, 1991). The steady-state concentrations of $^1O_2$ ($[^1O_2]_{ss}$) were estimated to be at the 10^{-14}–10^{-13} M level in natural waters, as determined with furfuryl alcohol (FFA) as a probe (Haag and Hoigne, 1986; Peterson et al., 2012; Scully et al., 1997). The $[^1O_2]_{ss}$ values are significantly different across water samples collected from different water bodies (lake, river, marine, and wastewater) due to the diversity of DOM (allochthonous or autochthonous) and the differences in DOM concentration (Haag and Hoigne, 1986). The DOM with low absorptivity and high quantum efficiency are generally of autochthonous origin, whereas those with high absorptivity and relatively low quantum efficiency are associated with allochthonous origin (Haag and Hoigne, 1986).

The formation of $^1O_2$ from isolated DOM was also well-investigated under simulated solar irradiation (Mayeda and Bard, 1973; Scurlock et al., 1995; Zhang et al., 2014; J. Wang et al., 2019; Y. Wang et al., 2019). The DOM of different sources exhibited disparate compositions and photochemical reactivity (Zhang et al., 2014; Maizel and Remucal, 2017). Besides, the Φ_{1O2} values from DOM that was isolated from coastal seawater were higher than those from freshwater (Suwannee River Fulvic Acid, SRFA) (J. Wang et al., 2019; Y. Wang et al., 2019). Zhou et al. (2017) found that the aromatic ketone groups in DOM are important sensitizers for the generation of $^1O_2$. Compared with allochthonous DOM, autochthonous DOM shows higher quantum yield of reactive intermediate (Wenk et al., 2011). Thus, the chemical composition of DOM, which is highly dependent on its source (terrestrial or aquatic) and formation processes (e.g., microbial and photochemical) (Leenheer and Croue, 2003; Helms et al., 2008), can significantly influence the formation of $^1O_2$.

Previous studies have investigated the correlations between the Φ_{1O2} of DOM and optical indices including absorption coefficients at specific wavelengths, absorbance ratio (E_2/E_3), slope radio (S_R), and spectral slope coefficient ($S_{300-600}$) (Du et al., 2018; Maizel and Remucal, 2017; McKay et al., 2017). Mckay et al. (2017) also reported that the Φ_{1O2} of DOM correlated negatively with the antioxidant activity, which indicates electron donating capacity. The optical and chemical properties of different DOM isolates are determined by their specific structure. The underlying relationships between the intrinsic structure characteristics of DOM and its Φ_{1O2} are still not fully understood. Analog structures of DOM from different sources (structures are shown in Fig. S1 and Table 1) were proposed based on experimental characterization and computer-assisted structure elucidation in previous studies (Diallo et al., 2003; Niederer and Goss, 2007; Wilson et al., 1987). Nowadays, the remarkable advancement of Fourier-transform ion cyclotron resonance mass spectrometry (FT-ICR-MS) and high-field nuclear magnetic resonance spectroscopy (NMR) has allowed more accurate identification of molecular composition of DOM (Zark and Dittmar, 2018; D. Li et al., 2019; C. Li et al., 2019), which makes it possible to analysis the photochemical properties of DOM at molecular level.

Thus, this study aims to construct the inherent relationships between the structure of DOM and the formation of $^1O_2$. The Φ_{1O2} values of 17 DOM-like model compounds and a commercial DOM (Suwannee River fulvic acid, SRFA) (structures are shown in Table 1) were determined in aqueous solutions, unlike the reported Φ_{1O2} values of DOM-like model compounds which were mainly determined in organic solvents (Nau and Scaiano, 1996) or with different probes (FFA, imidazole, and dimethylfuran) (Redmond and Gamlin, 1999). A quantitative structure-activity relationship (QSAR) model, as widely used to correlate molecular structures of organic compounds with their "reactivity" (Li et al., 2018; D. Li et al., 2019; C. Li et al., 2019; Gupta et al., 2016; Luo et al., 2017; Sudhakaran and Amy, 2013), was developed. The QSAR model was built by means of multiple linear regression (MLR) (J. Wang et al., 2019; Y. Wang et al., 2019), which is one of the most popular statistical algorithms. The highlight of this study is to further understand the $^1O_2$ formation mechanisms from DOM and predict the Φ_{1O2} of DOM from different sources.

2. Materials and methods

2.1. Chemicals

1,4-Naphthoquinone (99% purity), biacetyl (98% purity), acetophenone (98% purity), coumarin (98% purity), trans-cinnamic acid (99% purity), 7-hydroxycoumarin (98% purity), naphthalene (99% purity), 2-acetonaphthone (99% purity), 3-methoxyacetophenone (99% purity), benzophenone (99% purity), 1,4-benzoquinone (99% purity), riboflavin (98% purity), chlorohydroquinone (85% purity), gallic acid (99% purity) and furfuryl alcohol (98% purity) were obtained from J&K Scientific Ltd. (Beijing, China); dibenzoyl (99% purity), 4-methylbenzaldehyde (98% purity) were purchased from Tokyo Chemical Industry (Tokyo, Japan); duroquinone (97% purity) was obtained from Sigma-Aldrich (St. Louis, MO, U.S.A.). Organic solvents used in this study with chromatographical purity were obtained from TEDIA (Fairfield, OH, USA). Suwannee River fulvic acid (SRFA) was purchased from the International Humic Substances Society. Ultrapure water (PW, 18.2 MΩ) was obtained from a purification system produced by Chengdu Ultrapure Technology Co., Ltd. (Chengdu, China).

2.2. Light irradiation experiments

The light irradiation experiments were performed with a XPA-7 merry-go-round photochemical reactor (Xujiang Technology Co., Nanjing) equipped with a water-refrigerated system which kept the reaction temperature at 25 ± 1 °C. A 500 W medium-pressure mercury lamp with 290 nm filters (the filters blocked light below 290 nm) was used to mimic the UV-A, UV-B, and visible light portions of sunlight. The emission spectrum of the Hg lamp was detected with a TriOS-RAMSES spectroradiometer (TriOS GmbH, Germany), and the result is shown in Fig. S2. Furfuryl Alcohol (FFA) was used as the probe of $^1O_2$, and the initial concentrations of FFA and DOM-analogs were 50 μM and 10 mg/L, respectively. Besides, 0.1 mM methanol was added to the solution to quench hydroxyl radicals (•OH) produced during the irradiation. The reaction solution was introduced in quartz tubes and all the experiments were carried out in triplicate irradiated by 500 W medium-pressure mercury lamp. The details about solutions preparation were described in Text S2 in the Supporting information.

Table 1
Molecular structures of selected DOM-analogs.

Name	Structure	Name	Structure
1,4-Naphthoquinone*	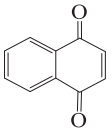	2-Acetonaphthone*	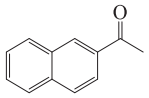
Biacetyl*		3-Methoxyacetophenone*	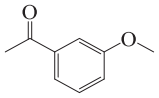
Dibenzoyl*	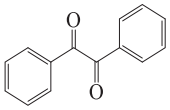	Duroquinone*	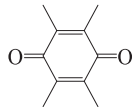
Acetophenone*	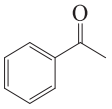	1,4-Benzoquinone*	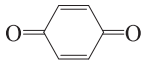
Coumarin*	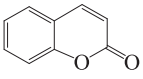	Benzophenon*	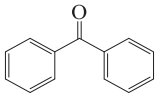
Trans-cinnamic acid*	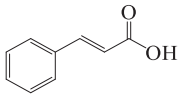	Gallic acid*	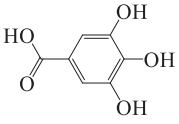
7-Hydroxycoumarin*	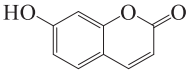	2-Chlorohydroquinone*	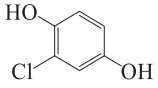
Naphthalene*	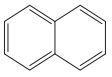	2-Hydroxy-4-methylbenzaldehyde*	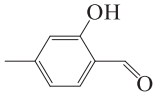
Riboflavin#	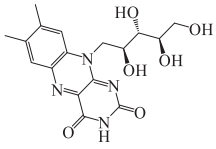	Suwannee River fulvic acid (SRFA)#	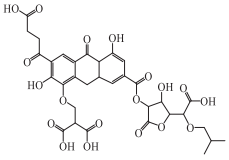

*Represents the compounds in the training set.
#Represents the compounds in the validation set.

2.3. Analytical methods

The spectra of DOM-analogs were collected by Hitachi-U2900. Quantitative analysis of FFA was performed on a Shimadzu LC-20A HPLC system (Shimadzu, Kyoto, Japan) equipped with UV–Vis detector and an Ultimate™ AQ-C18 column (250 mm × 4.6 mm, 5 μm, Welch Materials, Maryland, USA). FFA was eluted at a flow rate of 0.7 mL min^{-1} in 219 nm at 30 °C, and the mobile phase consisted of methanol and water at a ratio of 40:60 (v:v).

2.4. Calculation of singlet oxygen quantum yield

Quantum yield (Φ) is used to quantify the efficiency of photon utilization during photochemical reactions, as defined by means of the following equation (eq) (Kishino et al., 1986):

$$\Phi = \frac{\text{number of molecules take part in the photochemical reaction}}{\text{number of absorbed photons}} \quad (1)$$

According to Eq. (1), Φ of $^1O_2$ can be expressed as per Eq. (2), as the production rate of $^1O_2$ divided by the light absorption rate of the photosensitizers.

$$\Phi_{1O2} = \frac{R_{1O2}}{\sum_{\lambda} k_{X-a}(\lambda)[X]} \quad (2)$$

where R_{1O2} is the production rate of $^1O_2$ (M/s); $k_{X\text{-}a}(\lambda)$ is the characteristic light absorption rate of photosensitizer X (s^{-1}); [X] is the

concentration of photosensitizer ($mol \cdot L^{-1}$). Radiation wavelength range is 290 nm–500 nm.

$k_{X\text{-}a}$ (λ) can be calculated with the following equation (Zhou et al., 2018; Zhang et al., 2018a):

$$k_{X-a}(\lambda) = \frac{I_p \varepsilon_X(\lambda)\left(1-10^{-(\alpha(\lambda)+\varepsilon_X(\lambda)[X])z}\right)}{\varepsilon_X(\lambda)[X]z} \quad (3)$$

where I_p is the intensity of incident light ($Einstein \cdot s^{-1} \cdot cm^{-2}$); $\varepsilon_X(\lambda)$ is the molar absorptivity of the photosensitizer ($M^{-1} \cdot cm^{-1}$); z is the optical path (cm), which was calculated with the method described in Text S3.

FFA is often used as a probe to detect $^1O_2$, the production rate of $^1O_2$ is the same as the quenching rate, so the production rate of $^1O_2$ (R_{1O2}) is shown in Eq. (4):

$$R_{1O2} = R_{FFA}\frac{k_d + k_{FFA} \cdot [FFA]}{k_{FFA} \cdot [FFA]} \quad (4)$$

where R_{1O2} is the production rate of $^1O_2$, k_{FFA} (1.0×10^8 L mol^{-1} s^{-1}) is the second-order reaction rate constant for the reaction between FFA and $^1O_2$ (Appiani et al., 2017); R_{FFA} is the degradation rate of FFA (M/s), which was obtained by fitting the FFA concentration vs time; k_d is the quenching rate constant of $^1O_2$ upon collision with water molecules (2.5×10^5 s^{-1}); [FFA] is the initial concentration of FFA ($mol \cdot L^{-1}$).

$$\left[^1O_2\right]_{ss} = \frac{R_{1O2}}{k_{FFA} \cdot [FFA] + k_d} \quad (5)$$

The steady state concentration of $^1O_2$ ($[^1O_2]_{ss}$) can be calculated by means of Eq. (5). The value of Φ_{1O2} was obtained by replacing the numerator and denominator of Eq. (2) with Eqs. (4), and (3), respectively.

2.5. Development and evaluation of QSAR model

In this study, sixteen DOM-analogs were selected as the training set to construct the QSAR model for predicting $^1O_2$ quantum yield; two widely used excited triplet sensitizer—Riboflavin and SRFA were selected for the validating the QSAR model. The molecular structures of the 18 organic compounds are shown in Table 1. There are 17 aromatic compounds, among which five compounds contain an aromatic ketone group that is reported as an important sensitizer of $^1O_2$ (Sharpless, 2012); there are four compounds with quinone moieties that may also play important roles in the production of $^1O_2$ in NOM-enriched solutions (Zhou et al., 2017). Naphthalene and its derivatives were also considered important for the generation of $^1O_2$ (Klaper and Linker, 2015). Thus, we also selected naphthalene and substituted naphthalenes in the training set. In addition, biacetyl was proved to be the most useful sensitizer for all the oligomers, it was quenched by oxygen to yield $^1O_2$ (Dam et al., 1999). Halide ions are widespread in the ocean. They can induce the halogenation of DOM and influence the generation of $^1O_2$ by DOM (Glover and Rosario-Ortiz, 2013; Mendez-Diaz et al., 2014). Therefore, a chlorinated organic compound (2-chlorohydroquinone) was also selected as DOM-analog. The selected compounds in the dataset represent the diverse structures of DOM composition. The UV–vis absorption spectra of the sixteen DOM analogs, one widely used sensitizer (Riboflavin), and a commercial DOM (SRFA) are shown in Fig. S4. As can be seen from Fig. S4, the absorbance of each analog is >0 at λ > 290 nm, indicating their absorbing capacity under simulated sunlight irradiation.

Quantum chemical descriptors and DRAGON descriptors were used as independent variable to build a QSAR model. DRAGON descriptors can describe the structural diversity of the compounds and quantum chemical descriptors have clear physicochemical definition. Before calculating the DRAGON descriptors, the molecular structures of the 17 DOM-analogs and SRFA were optimized with the widely used B3LYP functional combined with the 6-31G+(d,p) basis set (D. Li et al., 2019; C. Li et al., 2019) using the Gaussian 09 program suite (Frisch et al., 2009). The solvent effects of water were considered by the integral equation formalism of the polarized continuum model (IEFPCM) based on the self-consistent-reaction-field method. Afterwards the DRAGON descriptors were calculated by the DRAGON software (version 7.0) (TALETE srl, Italy). The quantum chemical descriptors were obtained via calculations by both Gaussian 09 and Dragon 7.0. Sixteen DOM-analogs were used in the training set for the development of the model; the validation set was composed of the commercial DOM—SRFA, the widely used photosensitizer—riboflavin. Stepwise multiple linear regression (MLR) analysis was employed to construct the QSAR model. The more details are described in Text S1 in the supporting information.

3. Results and discussion

3.1. $^1O_2$ quantum yield of DOM-analogs and SRFA

Significant degradation of FFA was observed in solutions containing the DOM-analogs, sensitizers and SRFA under irradiation experiments (Fig. S3) (Zhou et al., 2019), implying the generation of $^1O_2$. The Φ_{1O2}, R_{1O2}, $[^1O_2]_{ss}$ were calculated with Eqs. (2), (4), and (5), the results are listed in Tables 2 and S1. The determined values of Φ_{1O2}, R_{1O2}, and $[^1O_2]_{ss}$ of the selected compounds range from $(0.54 \pm 0.23) \times 10^{-2}$ to $(62.03 \pm 2.97) \times 10^{-2}$, $(5.88 \pm 0.30) \times 10^{-8}$ M/s to $(1.89 \pm 0.08) \times 10^{-6}$ M/s, and $(2.31 \pm 0.12) \times 10^{-13}$ M to $(7.39 \pm 0.32) \times 10^{-12}$ M, respectively. Based on the Φ_{1O2} values, the sixteen DOM-analogs were divided into three classes (Table 2). The compounds in Class I are benzophenone, dibenzoyl and biacetyl with Φ_{1O2} values of $(62.03 \pm 2.97) \times 10^{-2}$, $(31.07 \pm 2.57) \times 10^{-2}$, and $(29.96 \pm 0.80) \times 10^{-2}$, respectively. The high Φ_{1O2} values of these three compounds are attributed to the extremely high ratios of energy transfer from their excited triplet states to oxygen compared with other deactivation pathways of the triplet states (Sawaki, 1985). Benzophenone and dibenzoyl are aromatic ketones with two benzene rings. Some compounds with similar structures were also reported to have high Φ_{1O2} values (Molins-Molina et al., 2017; Zhou et al., 2019). Biacetyl is the only aliphatic ketone among the selected DOM-analogs, of which the Φ_{1O2} value was also reported to be lower than the values for benzophenone and dibenzoyl and higher than for other aliphatic ketones such as 2-hexanone and 2-pentanone (Nau and Scaiano, 1996).

There are four compounds, including 3-methoxyacetophenone, acetophenone, 2-acetonaphthone, and trans-cinnamic acid, in class II with Φ_{1O2} values ranging from $(10.22 \pm 0.41) \times 10^{-2}$ to $(13.36 \pm 1.23) \times 10^{-2}$. The Φ_{1O2} value of 2-acetonaphthone, which is also an aromatic ketone with two benzene rings, is much lower compared to the value of benzophenone, indicating that a minor structural difference can lead to significant changes in the generation of $^1O_2$ from excited DOM. Besides 2-acetonaphthone, the two compounds with relatively high Φ_{1O2} values in class II are acetophenone and 3-methoxy acetophenone. These compounds are aromatic ketones with one benzene ring. The other DOM-analog in class II (trans-cinnamic acid) is an aromatic compound containing carbonyl groups.

The remaining compounds are included in class III with Φ_{1O2} values lower than 0.1. The compounds in class III are all aromatic compounds containing diverse functional groups, including ketones, quinones, phenols, aldehydes, carboxylic acids, and naphthalene. As can be seen in Tables 1 and 2, the Φ_{1O2} values of aromatic ketones are generally higher than those of other selected DOM-analogs except for biacetyl. Therefore, aromatic ketone groups in DOM may play an important role in the generation of $^1O_2$ under sunlight irradiation, which is in accordance with the results reported in previous studies (Gorman and Rodgers, 1986; Zhou et al., 2017). Based on the results reported above it can be concluded that the quinone and phenol groups in DOM have less influence on the generation of $^1O_2$ compared with aromatic ketone groups.

Table 2
Determined Φ_{1O2}, logΦ_{1O2} and predicted logΦ_{1O2} of DOM-analogs.

Class	Chemical	Φ_{1O2}[a] × 10^{-2}	Experimental logΦ_{1O2}	Predicted logΦ_{1O2}[b]
Class I	Benzophenone	62.03 ± 2.97	−0.21	−0.26
	Dibenzoyl	31.07 ± 2.57	−0.51	−0.27
	Biacetyl	29.96 ± 0.80	−0.52	−0.46
	Acetophenone	13.36 ± 1.23	−0.87	−1.03
Class II	2-Acetonaphthone	13.35 ± 1.61	−0.87	−1.01
	3-Methoxyacetophenone	12.15 ± 0.26	−0.92	−0.97
	Trans-cinnamic acid	10.22 ± 0.41	−0.99	−1.15
	Naphthalene	4.80 ± 1.66	−1.31	−1.19
	1,4-Naphthoquinone	3.82 ± 1.36	−1.38	−1.59
	Duroquinone	3.73 ± 0.39	−1.43	−1.45
	Gallic acid	2.93 ± 0.81	−1.53	−1.57
Class III	1,4-Benzoquinone	2.92 ± 0.10	−1.54	−1.60
	2-Chlorohydroquinone	2.64 ± 0.11	−1.58	−1.73
	Coumarin	1.68 ± 0.18	−1.77	−1.61
	7-Hydroxycoumarin	1.65 ± 0.25	−1.78	−1.77
	2-Hydroxy-4-methylbenzaldehyde	0.54 ± 0.23	−2.26	−1.82
	SRFA	1.61 ± 0.12	−1.79	−1.76
	Riboflavin	14.94 ± 2.39	−0.83	−0.93

[a] Positive and negative error range represents a 95% confidence interval, errors were calculated with three parallel data.
[b] logΦ_{1O2} values were predicted with the constructed QSAR model [Eq. (6)].

Unveiling the underlying mechanisms for the generation of $^1O_2$ from these DOM-analogs is of great significance for understanding the formation process of $^1O_2$ from DOM in natural waters.

The Φ_{1O2} values of riboflavin and SRFA are $(14.94 \pm 2.39) \times 10^{-2}$ and $(1.61 \pm 0.12) \times 10^{-2}$, respectively. Our Φ_{1O2} value of SRFA is close to the previously reported value of $(1.85 \pm 0.15) \times 10^{-2}$ (Zhang et al., 2014) and 2.02×10^{-2} (Mustafa and Rosario-Ortiz, 2013). The Φ_{1O2} values of Coumarin are $(1.68 \pm 0.18) \times 10^{-2}$, it is in the same order of magnitude with the reported value of 1.00×10^{-2} (Egorov et al., 1986). The determined Φ_{1O2} for SRFA is much lower than those of some analogs, especially the analogs in class I. This is because that the contribution of these groups (aromatic ketones) is low due to their small proportions in DOM. The Φ_{1O2} value of riboflavin is comparable with Φ_{1O2} values of aromatic ketones in class II. These results agree with the reported values in previous studies (Wilkinson et al., 1993; Maddigapu et al., 2010).

3.2. QSAR modeling

QSAR models for predicting values of Φ_{1O2} were constructed based on the determined Φ_{1O2} values and the calculated structural descriptors with the selected sixteen DOM-analogs. The QSAR model with the best performance is shown in Eq. (6):

$$\log\Phi_{1O2} = -5.861 + 0.658 \times CIC1 + 4.480 \times DLS\_cons - 1.327 \times Mor27in_t = 16, R^2 = 0.901, R^2_{adj} = 0.876, RMSE_t = 0.194, F = 34.447, Q^2_{Loo} = 0.839, P<0.0001 \quad (6)$$

n_t represents the number of the analogs in the training set; F represents test of variance; P represents the significance level of F. The model contains three molecular structural descriptors: the complementary information content index (neighborhood symmetry of 1-order, *CIC1*), the DRAGON consensus drug-like score (*DLS_cons*), and a 3D-MoRSE (Molecule Representation of Structures based on Electron diffraction) descriptor weighted by ionization potential (signal 27/weighted by ionization potential, *Mor27i*). The values of these molecular structural descriptors are listed in Table S2. The high value of R^2_{adj} (adjusted square of the determination coefficient) of 0.876 and the low $RMSE_t$ (root mean squared error) of 0.194 suggest that the established model had high goodness-of-fit; the high Q^2_{LOO} (leave-one-out cross-validated square of the determination coefficient) is indicative of the robustness of the model. The difference between R^2_{adj} and Q^2_{Loo} is <0.3 meaning that no overfitting occurred (Golbraikh and Tropsha, 2002). All VIF (variance inflation factors) of these descriptors are <1.21 (Table 3), therefore the model is free of multicollinearity. The logΦ_{1O2} values of the selected organic compounds and of SRFA as calculated with the constructed model (Eq. (6)), are listed in Table 2. As shown in Fig. 1, the predicted logΦ_{1O2} values agree well with the experimental values for all the DOM-analogs in the training set.

3.3. Mechanistic interpretation

As indicated by the *t*-test statistics and the corresponding significance level (*p* values) for the three descriptors (Table 3), *CIC1* is the most important factor for governing $^1O_2$ due its lowest *p* value of *t*-test. *CIC1* represents the maximum possible complexity of chemical structures and the topological information and it capable of characterizing chemical structure efficiently. *CIC1* was defined as Complementary information content of distance matrix based on chemical molecular structure (Basak et al., 1988). The logΦ_{1O2} values decrease with the decrease of *CIC1* which encodes the molecular complexity (Mercader et al., 2007). In the case of the structures for the DOM-analogs, *CIC1* is related to the presence of carbonyl, carboxyl, or hydroxyl groups. The presence of complex functional groups may increase the capability of light absorption that is essential for the generation of excited states of DOM and subsequent formation of $^1O_2$. *DLS_cons* represents the drug-like score that ranges from 0 to 1, in which a value of 1 indicates that a compound is a potential drug candidate (Lorenzo et al., 2015). Drug-like index was derived from the analysis of the whole Comprehensive Medicinal Chemistry database, it aims at reducing the number of compounds to be synthesized and tested, allowing the selection of compounds that have desired properties to be good drug candidates (Walters and Murcko, 2002). Besides, *DLS_cons* has often been used to describe the lipophilic character of organic compounds (Oksel et al., 2016). *DLS_cons* is positively correlated with logΦ_{1O2}, indicating that the hydrophobic functionalities in DOM exhibit an important role in the generation of $^1O_2$. It was previously reported that the apparent [$^1O_2$] in the hydrophobic microenvironment of DOM is much higher

Table 3
VIF, *t*-test values and significance level (*p* values) of descriptors in the model.

Descriptors	VIF	*t*	*p*
DLS_cons	1.085	6.201	<0.0001
CIC1	1.139	7.779	<0.00001
Mor27i	1.203	−5.869	<0.0001

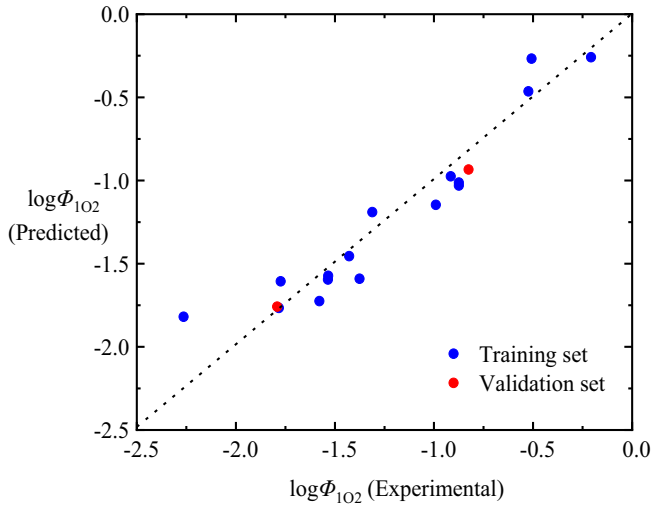

Fig. 1. Plot of predicted versus experimental logΦ_{1O2} values for the training and validation sets.

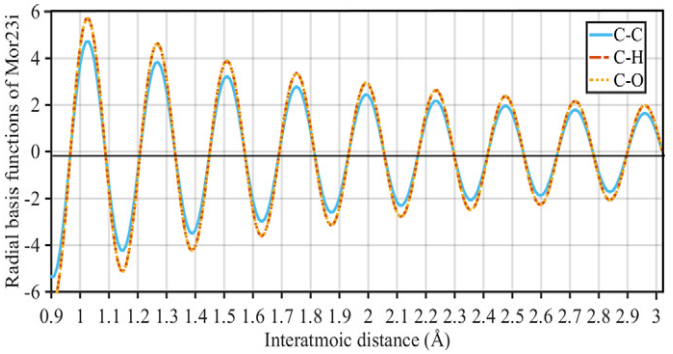

Fig. 2. Radial basis functions of Mor27i descriptor corresponding to different atomic pairs (interatomic distance, Å).

than the [$^1O_2$] in aqueous solutions (Latch and McNeill, 2006). This observation can be explained by the prominent contribution of hydrophobic groups in DOM to the generation of $^1O_2$.

Mor27i is a 3D-MoRSE descriptor which denotes representations of 3D molecular structures based on electron diffraction descriptors (Ahmadi et al., 2014). 3D-MoRSE descriptors were introduced in 1996 by Schuur, Selzer and Gasteiger with the motivation for encoding 3D-structure of a molecule by a fixed number of variables and were applied to computational chemistry (Schuur et al., 1996). The 3D-MoRSE descriptor was used in our QSAR models to describe the importance of atomic pairs by radial basis function (Devinyak et al., 2014). The radial basis function is a function whose value depends on the distance from the center point. The center point is the neutral atomic distance in this study. The radial basis function is often regarded as a simple neural network (Devinyak et al., 2014). It was calculated with Eq. (7):

$$f(r) = A_1 A_2 \frac{\sin 26r}{26r} \tag{7}$$

where A_1 and A_2 are corresponding carbon-scaled atomic ionization potential used as weights, r is the interatomic distance. The molecules with common atoms C, O and H. The carbon-scaled ionization potentials for these atoms are 11.2603, 13.6181 and 13.5984, respectively. As can be seen in Table 1, the selected DOM-analogs mainly contain C, H, and O atoms. Thus, the radial basis functions of Mor27i (which is weighted by ionization potential) corresponding to C—C, C—H, and C—O atomic pairs were calculated, as shown in Fig. 2. The most favorable atomic pairs are located at the distances about 1.03, 1.27, 1.51, 1.75, 1.99, 2.23, 2.48, and 2.72 Å (peaks), while the most detrimental pairs are located at 1.15, 1.39, 1.63, 1.87, 2.11, 2.36, 2.60, and 2.84 Å (troughs).

The bond lengths of potentially important atomic pairs in the generation of $^1O_2$ were obtained based on the optimized 3D configuration of the DOM-analogs. The bond length of C═O in all the selected compounds is about 1.23 Å which is close to one of the most favorable atomic pairs (1.27 Å), implying the important role of carbonyl groups in the generation of $^1O_2$ from DOM. This is in accordance with the experimental results that the compounds containing carbonyl group(s) have higher Φ_{1O2}. The bond length of C—O is about 1.37 Å, which is close to one of the most detrimental pairs (1.39 Å), indicating its negative influence on the generation of $^1O_2$ from DOM. Thus, the presence of C—O in the DOM-analogs (e.g., coumarin, 3-methoxyacetophenone, 7-hydroxycoumarin, 2-hydroxy-4-methylbenzaldehyde, and gallic acid) that also contain at least one carbonyl group is the reason for their relatively low value of Φ_{1O2}. The high Φ_{1O2} [$(10.22 \pm 0.41) \times 10^{-2}$] for trans-cinnamic acid (p*K*a: 4.44) is attributed to its dissociation in experimental solutions which leads to the formation of two C═O bonds with a bond length of about 1.27 Å.

3.4. Applicability domain and model validation

3.4.1. Applicability domain

The descriptor space of the QSAR model is depicted in Fig. 3. It can be seen that all the DOM-analogs and SRFA are in the domain, and none of them is particularly influential in the model space. This implies that the training set compounds are of diverse structures. According to the molecular structures of the compounds in the training set, the applicability domain of the developed MLR model covers diverse functional groups, such as carbonyl, hydroxyl, and carboxyl group, as well as chlorine, etc.

The standardized residual values for the sixteen compounds in the training set and two compounds in the validation set are all less than |3| (Fig. 4), and all the leverage values (h) are lower than their warning leverage value (h^*). Leverage, is widely used to evaluate the influence of the particular chemical's structure on the model, and is suitable for evaluating the degree of extrapolation of a QSAR model (Gramatica, 2007). From Fig. 4 we know that there are no outliers in either the training set or the validation set of the model. Thus, it can be inferred that the developed model can be employed to predict Φ_{1O2} values of the DOM and DOM-analogs. As far as we know, this QSAR model with the defined applicability domain is the first of its kind with regard to predicting Φ_{1O2} of DOM and DOM-analogs.

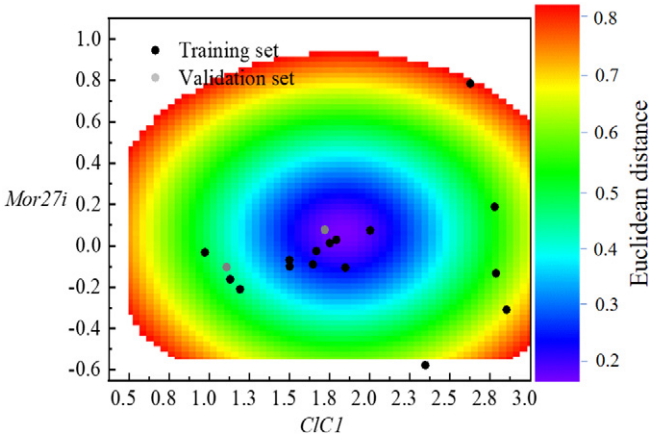

Fig. 3. The molecular descriptor space of the developed QSAR model, as characterized by the Euclidean distance-based approach. *ClC1*: complementary information content index (neighborhood symmetry of 1-order); *Mor27i*: 3D-MoRSE descriptors weighted by ionization potential (signal 27/weighted by ionization potential).

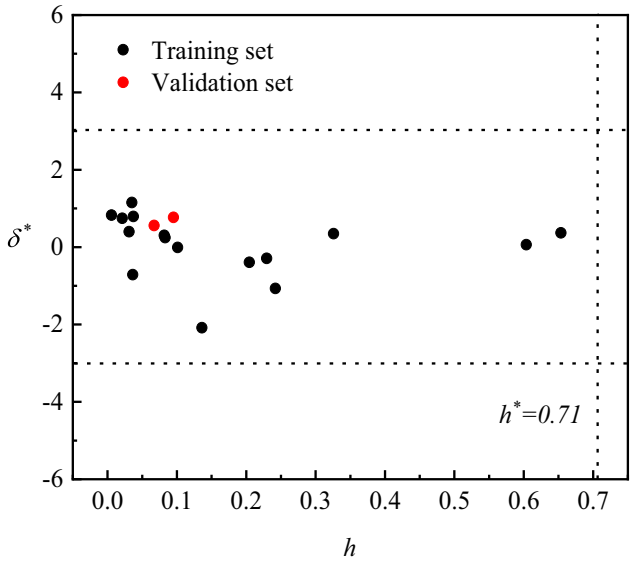

Fig. 4. Williams plots of standardized residuals (δ^*) versus leverage values (h) (h^* is the warning leverage value).

3.4.2. Validation of the constructed QSAR model

SRFA, a widely used commercial DOM with a modeled molecular structure (Table 1), was selected to validate the predictive capability of the constructed QSAR model. As can be seen in Figs. 1 and 3, SRFA lies in the applicability domain of the established QSAR model. The predicted logΦ_{1O2} of SRFA is −1.76, which is reasonable compared to the experimentally determined value (−1.79). This shows that the established model is of excellent predictive performance. Model prediction depends on the structure of the actual DOM. Whether the structure of DOM from different sources can be accurately obtained will determine the accuracy of the prediction.

The predictive capability of the constructed QSAR model was also confirmed by predicting the logΦ_{1O2} values of the widely used sensitizer—riboflavin, it contain also other heteroatoms besides O. The predicted logΦ_{1O2} value of riboflavin is −0.93, which is also in good agreement with the experimentally determined values (Table 2 and Fig. 1). The predicted Φ_{1O2} value of riboflavin (11.64×10^{-2}) is lower than the experimentally determined value of 14.94×10^{-2}. This shows that the presence of nitrogen atoms in DOM may promote the generation of $^1O_2$ from DOM.

4. Conclusions

The results of this study showed that the selected DOM-analogs are efficient $^1O_2$ sensitizers and the generation of $^1O_2$ from DOM-analogs is structure-dependent. The constructed MLR-QSAR model exhibited satisfactory goodness-of-fit, robustness, and good predictability. Meanwhile, the QSAR model is helpful for the mechanistic interpretation of $^1O_2$ generation from DOM. The presence of carbonyl groups is positively contributed to the generation of $^1O_2$ from DOM. Additionally, the generation of $^1O_2$ is mainly determined by the hydrophobicity and molecular complexity of DOM. The heteroatoms besides O in DOM can also affect the generation of $^1O_2$. In general, the developed QSAR model is beneficial for mechanistic interpretation of the generation of $^1O_2$ and can be potentially used for the prediction of the photochemical activity of DOM isolates. However, the accurate prediction of Φ_{1O2} from DOM is faced with great gap as the molecular structures of different DOM types still provides an analytical challenge. The prediction accuracy of this model highly relies on the reliability of modeled DOM molecular structures. However, it is possible to determine the detailed structures of DOM isolates from diverse locations with the development of new analytic equipment and methods.

Declaration of competing interest

The authors declare that they have no known competing financial interests or personal relationships that could have appeared to influence the work reported in this paper.

Acknowledgements

This study was supported by the National Natural Science Foundation of China (21707017 and 41877364) and the Jilin Province Science and Technology Development Projects (20180520079JH).

Appendix A. Supplementary data

Supplementary data to this article can be found online at https://doi.org/10.1016/j.scitotenv.2019.136450.

References

Agnez-Lima, L.F., Melo, J.T.A., Silva, A.E., Oliveira, A.H.S., Timoteo, A.R.S., Lima-Bessa, K.M., Martinez, G.R., Medeiros, M.H.G., Di Mascio, P., Galhardo, R.S., Menck, C.F.M., 2012. DNA damage by singlet oxygen and cellular protective mechanisms. Mutat. Res. 751, 15–28.

Ahmadi, S., Khazaei, M.R., Abdolmaleki, A., 2014. Quantitative structure-property relationship study on the intercalation of anticancer drugs with ct-DNA. Med. Chem. Res. 23, 1148–1161.

Appiani, E., Ossola, R., Latch, D.E., Erickson, P.R., McNeill, K., 2017. Aqueous singlet oxygen reaction kinetics of furfuryl alcohol: effect of temperature, pH, and salt content. Environ. Sci. Proc. Impacts. 19 (4), 507–516.

Basak, S.C., Magnuson, V.R., Niemi, G.J., Regal, R.R., 1988. Determining structural similarity of chemicals using graph-theoretic indices. Disc. Appl. Math. 19, 1744.

Cadet, J., Douki, T., Ravanat, J.L., 2008. Oxidatively generated damage to the guanine moiety of DNA: mechanistic aspects and formation in cells. Acc. Chem. Res. 41, 1075–1083.

Czaplicka, M., 2006. Photo-degradation of chlorophenols in the aqueous solution. J. Hazard. Mater. 134 (1–3), 45–59.

Dam, N., Scurlock, R.D., Wang, B., Ma, L., Sundahl, M., Ogilby, P.R., 1999. Singlet oxygen as a reactive intermediate in the photodegradation of phenylenevinylene oligomers. Chem. Mater. 11 (5), 1302–1305.

Devinyak, O., Havrylyuk, D., Lesyk, R., 2014. 3D-MoRSE descriptors explained. J. Mol. Graphics Modell. 54, 194–203.

Diallo, M.S., Simpson, A., Gassman, P., 2003. 3-D structural modeling of humic acids through experimental characterization, computer assisted structure elucidation and atomistic simulations. 1. Chelsea soil humic acid. Environ. Sci. Technol. 37 (9), 1783–1793.

Du, Z., He, Y., Fan, J., Fu, H., Zheng, S., Xu, Z., Qu, X., Kong, A., Zhu, D., 2018. Predicting apparent singlet oxygen quantum yields of dissolved black carbon and humic substances using spectroscopic indices. Chemosphere 194, 405–413.

Egorov, S.Y., Krasnovsky, A.A., Sukhorukov, V.L., Potapenko, A.Y., 1986. Furocoumarin-photosensitized formation of singlet oxygen in aqueous and alcohol solution. Biophysics 31, 172–174.

Foote, C.S., 1991. Definition of type-I and type-II photosensitized oxidation. Photochem. Photobiol. 54, 659.

Frisch, M.J., Trucks, G.W., Schlegel, H.B., Scuseria, G.E., Robb, M.A., Cheeseman, J.R., Scalmani, G., Barone, V., Mennucci, B., Petersson, G.A., Nakatsuji, H., Caricato, M., Li, X., Hratchian, H.P., Izmaylov, A.F., Bloino, J., Zheng, G., Sonnenberg, J.L., Hada, M., Ehara, M., Toyota, K., Fukuda, R., Hasegawa, J., Ishida, M., Nakajima, T., Honda, Y., Kitao, O., Nakai, H., Vreven, T., Montgomery Jr., J.A., Peralta, J.E., Ogliaro, F., Bearpark, M., Heyd, J.J., Brothers, E., Kudin, K.N., Staroverov, V.N., Kobayashi, R., Normand, J., Raghavachari, K., Rendell, A., Burant, J.C., Iyengar, S.S., Tomasi, J., Cossi, M., Rega, N., Millam, J.M., Klene, M., Knox, J.E., Cross, J.B., Bakken, V., Adamo, C., Jaramillo, J., Gomperts, R., Stratmann, R.E., Yazyev, O., Austin, A.J., Cammi, R., Pomelli, C., Ochterski, J.W., Martin, R.L., Morokuma, K., Zakrzewski, V.G., Voth, G.A., Salvador, P., Dannenberg, J.J., Dapprich, S., Daniels, A.D., Farkas, O., Foresman, J.B., Ortiz, J.V., Cioslowski, J., Fox, D.J., 2009. Gaussian 09, Revision A.01. Gaussian, Inc., Wallingford, CT.

Glover, C.M., Rosario-Ortiz, F.L., 2013. Impact of halides on the photoproduction of reactive intermediates from organic matter. Environ. Sci. Technol. 47 (24), 13949–13956.

Golbraikh, A., Tropsha, A., 2002. Beware of q2! J. Mol. Graphics Modell. 20, 269–276.

Gorman, A.A., Rodgers, M.A.J., 1986. The quenching of aromatic ketone triplets by oxygen: competing singlet oxygen and biradical formation? J. Am. Chem. Soc. 108 (17), 5074–5078.

Gramatica, P., 2007. Principles of QSAR models validation: internal and external. QSAR Comb. Sci. 26, 694–701.

Gupta, S., Basant, N., Mohan, D., Singh, K.P., 2016. Modeling the reactivities of hydroxyl radical and ozone towards atmospheric organic chemicals using quantitative

structure-reactivity relationship approaches. Environ. Sci. Pollut. Res. 23, 14034–14046.
Haag, W., Hoigne, J., 1986. Singlet oxygen in surface waters. 3. Photochemical formation and steady-state concentrations in various types of waters. Environ. Sci. Technol. 20, 341–348.
Helms, J.R., Stubbins, A., Ritchie, J.D., Minor, E.C., Kieber, D.J., Mopper, K., 2008. Absorption spectral slopes and slope ratios as indicators of molecular weight, source, and photobleaching of chromophoric dissolved organic matter. Limnol. Oceanogr. 53 (3), 955–969.
Karpuzcu, M.E., McCabe, A.J., Arnold, W.A., 2016. Phototransformation of pesticides in prairie potholes: effect of dissolved organic matter in triplet-induced oxidation. Environ. Sci. Proc. Impacts. 18 (2), 237–245.
Kishino, M., Okami, N., Takahashi, M., Ichimura, S.E., 1986. Light utilization efficiency and quantum yield of phytoplankton in a thermally stratified sea. Limnol. Oceanogr. 31 (3), 557–566.
Klaper, M., Linker, T., 2015. New singlet oxygen donors based on naphthalenes: synthesis, physical chemical data, and improved stability. Chem. Eur. J. 21 (23), 8569–8577.
Latch, D.E., McNeill, K., 2006. Microheterogeneity of singlet oxygen distributions in irradiated humic acid solutions. Science 311, 1743–1747.
Leenheer, J.A., Croue, J.P., 2003. Characterizing aquatic dissolved organic matter. Environ. Sci. Technol. 37 (1), 18A–26A.
Li, C., Wei, G., Chen, J., Zhao, Y., Zhang, Y., Su, L., Qin, W., 2018. Aqueous OH radical reaction rate constants for organophosphorus flame retardants and plasticizers: experimental and modeling studies. Environ. Sci. Technol. 52, 2790–2799.
Li, D., Yang, X., Zhou, Z., J, B., Tawfikd, A., Zhaoa, S., Meng, F., 2019a. Molecular traits of phenolic moieties in dissolved organic matter: linkages with membrane fouling development. Environ. Int. 133, 105–202.
Li, C., Zheng, S., Li, T., Chen, J., Zhou, J., Su, L., Zhang, Y., Crittenden, J.C., Zhu, S., Zhao, Y., 2019b. Quantitative structure-activity relationship models for predicting reaction rate constants of organic contaminants with hydrated electrons and their mechanistic pathways. Water Res. 151, 468–477.
Lorenzo, V.P., Barbosa Filho, J.M., Scotti, L., Scotti, M.T., 2015. Combined structure- and ligand-based virtual screening to evaluate caulerpin analogs with potential inhibitory activity against monoamine oxidase B. Rev. Bras. Farmacogn. 25 (6), 690–697.
Luo, X., Yang, X., Qiao, X., Wang, Y., Chen, J., Wei, X., Peijnenburg, W.J.G.M., 2017. Development of a QSAR model for predicting aqueous reaction rate constants of organic chemicals with hydroxyl radicals. Environ. Sci. Proc. Impacts. 19, 350–356.
Maddigapu, P.R., Bedini, A., Minero, C., Maurino, V., Vione, D., Brigante, M., Mailhot, G., Sarakha, M., 2010. The pH-dependent photochemistry of anthraquinone-2-sulfonate. Photochem. Photobiol. Sci. 9 (3), 323–330.
Maizel, A.C., Remucal, C.K., 2017. Molecular composition and photochemical reactivity of size fractionated dissolved organic matter. Environ. Sci. Technol. 51 (4), 2113–2123.
Mayeda, E.A., Bard, A.J., 1973. Production of singlet oxygen in electrogenerated radical ion electron transfer reactions. J. Am. Chem. Soc. 95 (19), 6223–6226 1973.
McKay, G., Huang, W., Romera-Castillo, C., Crouch, J.E., Rosario-Ortiz, F.L., Jaffe, R., 2017. Predicting reactive intermediate quantum yields from dissolved organic matter photolysis using optical properties and antioxidant capacity. Environ. Sci. Technol. 51, 5404–5413.
Mendez-Diaz, J.D., Shimabuku, K.K., Ma, J., Enumah, Z.O., Pignatello, J.J., Mitch, W.A., Dodd, M.C., 2014. Sunlight-driven photochemical halogenation of dissolved organic matter in seawater: a natural abiotic source of organobromine and organoiodine. Environ. Sci. Technol. 48 (13), 7418–7427.
Mercader, A.G., Duchowicz, P.R., Sanservino, M.A., Fernandez, F.M., Castro, E.A., 2007. QSPR analysis of fluorophilicity for organic compounds. J. Fluor. Chem. 128, 484–492.
Molins-Molina, O., Bresolí-Obach, R., Garcia-Lainez, G., Andreu, I., Nonell, S., Miranda, M.A., Jiménez, M.C., 2017. Singlet oxygen production and in vitro phototoxicity studies on fenofibrate, mycophenolate mofetil, trifusal, and their active metabolites. J. Phys. Org. Chem. 30 (9), 3722.
Mostafa, S., Rosario-Ortiz, F.L., 2013. Singlet oxygen formation from wastewater organic matter. Environ. Sci. Technol. 47 (15), 8179–8186.
Nau, W.M., Scaiano, J.C., 1996. Oxygen quenching of excited aliphatic ketones and diketones. J. Phys. Chem. B 100 (27), 11360–11367.
Nelson, K.L., Boehm, A.B., Davies-Colley, R.J., Dodd, M.C., Kohn, T., Linden, K.G., Liu, Y., Maraccini, P.A., McNeill, K., Mitch, W.A., Nguyen, T.H., Parker, K.M., Rodriguez, R.A., Sassoubre, L.M., Silverman, A.I., Wigginton, K.R., Zepp, R.G., 2018. Sunlight-mediated inactivation of health-relevant microorganisms in water: a review of mechanisms and modeling approaches. Environ. Sci. Proc. Impacts. 20, 1089–1122.
Niederer, C., Goss, K.U., 2007. Quantum chemical modeling of humic acid/air equilibrium partitioning of organic vapors. Environ. Sci. Technol. 41 (10), 3646–3652.
Niu, X., Busetti, F., Langsa, M., Croué, J.-P., 2016. Roles of singlet oxygen and dissolved organic matter in self-sensitized photo-oxidation of antibiotic norfloxacin under sunlight irradiation. Water Res. 106, 214–222.
Oksel, C., Winkler, D.A., Ma, C.Y., Wilkins, T., Wang, X.Z., 2016. Accurate and interpretable nanoSAR models from genetic programming-based decision tree construction approaches. Nanotoxicology 1–44.
Peterson, B.M., McNally, A.M., Cory, R.M., Thoemke, J.D., Cotner, J.B., McNeill, K., 2012. Spatial and temporal distribution of singlet oxygen in Lake Superior. Environ. Sci. Technol. 46, 7222–7229.
Redmond, R.W., Gamlin, J.N., 1999. A compilation of singlet oxygen yields from biologically relevant molecules. Photochem. Photobiol. 70 (4), 391–475.
Sawaki, Y., 1985. Mechanistic study on the photo-oxidation of α-diketones: interaction of triplet α-diketones with oxygen. Tetrahedron 41 (11), 2199–2205.
Schuur, J.H., Selzer, P., Gasteiger, J., 1996. The coding of the three-dimensional structure of molecules by molecular transforms and its application to structure–spectra correlations and studies of biological activity. J. Chem. Inf. Comput. Sci. 36, 334–344.
Scully, N., Vincent, W., Lean, D., Cooper, W., 1997. Implications of ozone depletion for surface-water photochemistry: sensitivity of clear lakes. Aquat. Sci. 59, 260–274.
Scurlock, R.D., Wang, B., Ogilby, P.R., Sheats, J.R., Clough, R.L., 1995. Singlet oxygen as a reactive intermediate in the photodegradation of an electroluminescent polymer. J. Am. Chem. Soc. 1995 117 (41), 10194–10202.
Sharpless, C.M., 2012. Lifetimes of triplet dissolved natural organic matter (DOM) and the effect of NaBH4 reduction on singlet oxygen quantum yields: implications for DOM photophysics. Environ. Sci. Technol. 46 (8), 4466–4473.
Straight, R., Spikes, J., 1985. Photosensitized oxidation of biomolecules. In: Frimer, A.A. (Ed.), Singlet O2. 4. CRC Press, Boca Raton, pp. 91–143.
Sudhakaran, S., Amy, G.L., 2013. QSAR models for oxidation of organic micropollutants in water based on ozone and hydroxyl radical rate constants and their chemical classification. Water Res. 47, 1111–1122.
Vione, D., Minella, M., Maurino, V., Minero, C., 2014. Indirect photochemistry in sunlit surface waters: photoinduced production of reactive transient species. Chem. Eur. J. 20, 10590–10606.
Walters, W.P., Murcko, M.A., 2002. Prediction of 'drug-likeness'. Adv. Drug Deliv. Rev. 54, 255–271.
Wang, J., Chen, J., Qiao, X., Zhang, Y., Uddin, M., Guo, Z., 2019a. Disparate effects of DOM extracted from coastal seawaters and freshwaters on photodegradation of 2,4-dihydroxybenzophenone. Water Res. 151, 280–287.
Wang, Y., Chen, J., Tang, W., Xia, D., Liang, Y., Li, X., 2019b. Modeling adsorption of organic pollutants onto single-walled carbon nanotubes with theoretical molecular descriptors using MLR and SVM algorithms. Chemosphere 214, 79–84.
Wenk, J., Von Gunten, U., Canonica, S., 2011. Effect of dissolved organic matter on the transformation of contaminants induced by excited triplet states and the hydroxyl radical. Environ. Sci. Technol. 45, 1334–1340.
Wilkinson, F., Helman, W.P., Ross, A.B., 1993. Quantum yields for the photosensitized formation of the lowest electronically excited singlet state of molecular oxygen in solution. J. Phys. Chem. Ref. Data 22 (1), 113–262.
Wilson, M.A., Vassallo, A.M., Perdue, E.M., Reuter, J.H., 1987. Compositional and solid-state nuclear-magnetic-resonance study of humic and fulvic-acid fractions of soil organic-matter. Anal. Chem. 59 (4), 551–558.
Xie, Q., Chen, J., Zhao, H., Qiao, X., Cai, X., Li, X., 2013. Different photolysis kinetics and photooxidation reactivities of neutral and anionic hydroxylated polybrominated diphenyl ethers. Chemosphere 90, 188–194.
Zark, M., Dittmar, T., 2018. Universal molecular structures in natural dissolved organic matter. Nat. Commun. 9 (1), 1–8 2018.
Zepp, R., Wolfe, N., Baughman, G., Hollis, R., 1977. Singlet oxygen in natural waters. Nature 267, 421–423.
Zhang, D., Yan, S., Song, W., 2014. Photochemically induced formation of reactive oxygen species (ROS) from effluent organic matter. Environ. Sci. Technol. 48 (21), 12645–12653.
Zhang, Y., Wang, J., Chen, J., Zhou, C., Xie, Q., 2018a. Phototransformation of 2,3-dibromopropyl-2,4,6-tribromophenyl ether (DPTE) in natural waters: important roles of dissolved organic matter and chloride ion. Environ. Sci. Technol. 52 (18), 10490–10499.
Zhang, Y., Zhou, Y., Qu, J., Chen, J., Zhao, J., Lu, Y., Li, C., Xie, Q., Peijnenburg, W.J.G.M., 2018b. Unveiling the important roles of coexisting contaminants on photochemical transformations of pharmaceuticals: fibrate drugs as a case study. J. Hazard. Mater. 358, 216–221.
Zhou, H., Lian, L., Yan, S., Song, W., 2017. Insights into the photo-induced formation of reactive intermediates from effluent organic matter: the role of chemical constituents. Water Res. 112, 120–128.
Zhou, C., Chen, J., Xie, H., Zhang, Y., Li, Y., Wang, Y., Xie, Q., Zhang, S., 2018. Modeling photodegradation kinetics of organic micropollutants in water bodies: a case of the yellow river estuary. J. Hazard. Mater. 349, 60.
Zhou, Y., Zhao, J., Zhang, Y., Qu, J., Li, C., Qin, W., Zhao, Y., Chen, J., Peijnenburg, W.J.G.M., 2019. Trace amounts of fenofibrate acid sensitize the photodegradation of bezafibrate in effluents: mechanisms, degradation pathways, and toxicity evaluation. Chemosphere 235, 900–907.